Quantum oscillations and quasiparticle properties of thin film Sr_2RuO_4

Yawen Fang,[1] Hari P. Nair,[2] Ludi Miao,[1] Berit Goodge,[3] Nathaniel J. Schreiber,[2] Jacob P. Ruf,[1] Lena F. Kourkoutis,[3,4] Kyle M. Shen,[1,4] Darrell G. Schlom,[2,4,5] and B. J. Ramshaw[1,*]

[1]*Laboratory of Atomic and Solid State Physics, Cornell University, Ithaca, New York 14853, USA*
[2]*Department of Materials Science and Engineering, Cornell University, Ithaca, New York 14853, USA*
[3]*School of Applied and Engineering Physics, Cornell University, Ithaca, New York 14853, USA*
[4]*Kavli Institute at Cornell for Nanoscale Science, Ithaca, New York 14853, USA*
[5]*Leibniz-Institut für Kristallzüchtung, Max-Born-Strasse 2, 12489 Berlin, Germany*

(Received 28 February 2021; revised 17 June 2021; accepted 14 July 2021; published 30 July 2021)

We measure the Shubnikov–de Haas effect in thin-film Sr_2RuO_4 grown on an $(LaAlO_3)_{0.29}$-$(SrAl_{1/2}Ta_{1/2}O_3)_{0.71}$ substrate. We detect all three known Fermi surfaces and extract the Fermi surface volumes, cyclotron effective masses, and quantum lifetimes. We show that the electronic structure is nearly identical to that of single-crystal Sr_2RuO_4, and that the quasiparticle lifetime is consistent with the T_c of comparably clean, single-crystal Sr_2RuO_4. Unlike single-crystal Sr_2RuO_4, where the quantum and transport lifetimes are roughly equal, we find that the transport lifetime is 1.3 ± 0.1 times longer than the quantum lifetime. This may suggest that extended (rather than point) defects could be the dominant source of quasiparticle scattering in these films. To test this hypothesis, we perform cross-sectional scanning transmission electron microscopy and find that out-of-phase boundaries extending the entire thickness of the film occur with a density that is consistent with the quantum mean free path. The long quasiparticle lifetimes make these films ideal for studying the unconventional superconducting state in Sr_2RuO_4 through the fabrication of devices—such as planar tunnel junctions and superconducting quantum interference devices.

DOI: 10.1103/PhysRevB.104.045152

I. INTRODUCTION

Sr_2RuO_4 was long thought to be a p-wave superconductor, but recently revised nuclear magnetic resonance (NMR) measurements find a substantial decrease in the Knight shift across the superconducting transition temperature T_c [1], essentially ruling out all spin-triplet pairing states. While the details of the superconducting state are far from settled [2,3], it appears that single-crystal Sr_2RuO_4 is not a $p_x + ip_y$ superconductor. It may be possible, however, that multiple superconducting order parameters lie nearby in energy [4,5], suggesting that the application of the right tuning parameter could push Sr_2RuO_4 into a p-wave state. Uniaxial strain along the [100] direction has been shown to strongly enhance T_c [6], and while there is no signature of p-wave superconductivity under strain in single crystals, these measurements suggest that strain is a good parameter for manipulating the superconducting state of Sr_2RuO_4.

Unlike single-crystal strain experiments, which are necessarily uniaxial or hydrostatic, thin films can be strained biaxially through substrate engineering. For example, using five different substrates, the authors of Ref. [7] showed that the γ Fermi surface sheet of Sr_2RuO_4 (and the closely related compound Ba_2RuO_4) can be driven through the Brillouin zone boundary. These films, however, were not superconducting, and for decades the growth of superconducting thin-film Sr_2RuO_4 has been a major challenge in the oxide thin film community [8]. The difficulty stems from the extreme sensitivity of Sr_2RuO_4 to even minute levels of disorder—single crystals with greater than 1 μOhm-cm residual resistivity do not superconduct [9]. With the advent of Sr_2RuO_4 films that are clean enough to show superconductivity on many different substrates [10–12], it is worth investigating whether the superconductivity is a product of film quality, substrate strain, or both, how the quasiparticle properties are modified by the substrate, and what types of defects might be limiting the quasiparticle mean free path.

II. EXPERIMENT

A 100-nm-thick film of Sr_2RuO_4 was grown via molecular-beam epitaxy on an $(LaAlO_3)_{0.29}$-$(SrAl_{1/2}Ta_{1/2}O_3)_{0.71}$ (LSAT) substrate with the tetragonal c-axis perpendicular to the substrate surface. This substrate imposes a 0.045% tensile strain (a dilation of the tetragonal unit cell) at low temperature. The growth procedure is described in Refs. [10,13,14]. Devices for measuring electrical resistivity in the ab-plane were fabricated using standard photolithography techniques and ion milling [see Fig. 1(a)]. Devices were contacted by sputtering a 5-nm titanium adhesion layer followed by 25 nm of platinum. The temperature dependence of the in-plane resistivity, ρ_{xx}, reveals a high-quality device, with a RRR of 106 and a superconducting T_c of 1.05 K [RRR is defined

*To whom correspondence should be addressed: bradramshaw@cornell.edu

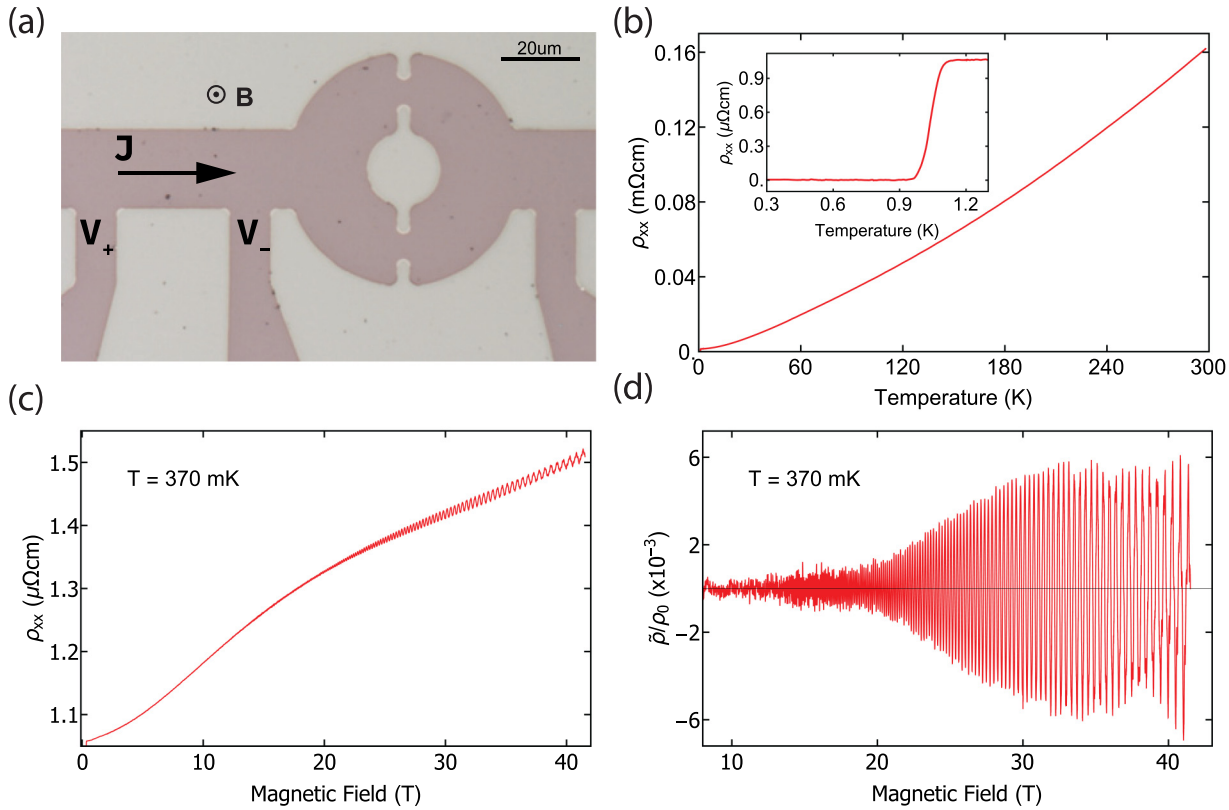

FIG. 1. Shubnikov–de Haas oscillations in Sr_2RuO_4 on LSAT. (a) The Sr_2RuO_4 transport device patterned from a thin film of Sr_2RuO_4 grown on an LSAT substrate. The structure to the right of the voltage contacts was not part of this experiment. (b) Resistivity as a function temperature: The inset shows the superconducting transition with a midpoint of $T = 1.05$ K. (c) Resistivity as a function of magnetic field. (d) The normalized oscillatory component of the resistivity.

as $R(298K)/R(T_c)$, with T_c measured at the midpoint of the transition—see Fig. 1(b)].

Quantum oscillation measurements were performed in the 41 T resistive magnet at the National High Magnetic Field Lab in Tallahassee. The magnetic field was oriented parallel to the crystallographic c-axis—perpendicular to the plane of the device. The temperature was controlled at fixed intervals between 370 mK and 2.2 K in a helium-3 cryostat. The sample resistance was measured in a standard 4-point contact geometry using a Stanford Research 860 lock-in amplifier, with a Stanford Research CS 580 Voltage Controlled Current Source and a Stanford Research SR560 low-noise preamplifier. The current through the sample was $I_{pp} = 150\,\mu$A. The magnetic field was swept at a rate of 0.2 T/min, and the time constant of the lock-in amplifier was set to 1 s. The slow sweep rate ensured that the high-frequency oscillations were not washed out by the time constant of the lock-in amplifier.

Figure 1(c) presents the magnetic field dependence of the resistivity at 370 mK. The total resistivity $\rho(B)$ is composed of two parts: a nonoscillatory background $\rho_0(B)$, which we obtain by fitting a smooth polynomial to the data, and an oscillatory component $\tilde{\rho}(B)$. The oscillatory fraction of the resistivity, $\tilde{\rho}/\rho_0$ [15], is given by

$$\frac{\tilde{\rho}}{\rho_0} = \left(\frac{\rho}{\rho_0} - 1\right) \tag{1}$$

and is plotted in Fig. 1(d). Shubnikov–de Haas oscillations are clearly visible above 15 T, with multiple frequencies visible above 35 T [see Fig. 2(a) and the supplementary information for details about the data analysis [16]].

III. ANALYSIS

We analyze the temperature and field dependence of the Shubnikov–de Haas oscillations to determine the Fermi surface area, the quasiparticle effective mass, and the quasiparticle mean free path, for all three sheets of the Fermi surface. The fast Fourier transform (FFT) of $\tilde{\rho}/\rho_0$, shown in Fig. 2(b), has clear contributions from all three known pieces of Fermi surface, labeled α, β, and γ, in accordance with previous studies [17]. Harmonics from the α pocket are visible up to the fifth order—another indication of high sample quality, as harmonic amplitude is dampened out exponentially with increasing harmonic number.

The Fermi surface area A_k is obtained from the quantum oscillation frequency F through the Onsager relation $A_k = (2\pi e/\hbar)F$. LSAT substrates apply a relatively small amount of tensile strain on the Sr_2RuO_4 films, and thus we expect the Fermi surface area of Sr_2RuO_4 films to be close to what is measured in single-crystal Sr_2RuO_4. This is what we observe: Within our experimental resolution, the three Fermi surfaces of Sr_2RuO_4 grown on LSAT have the same area as those reported for single crystals (a comparison is shown in Table I). This is consistent with the relatively small, 0.045% A_{1g} strain imposed by LSAT to the film at low temperature.

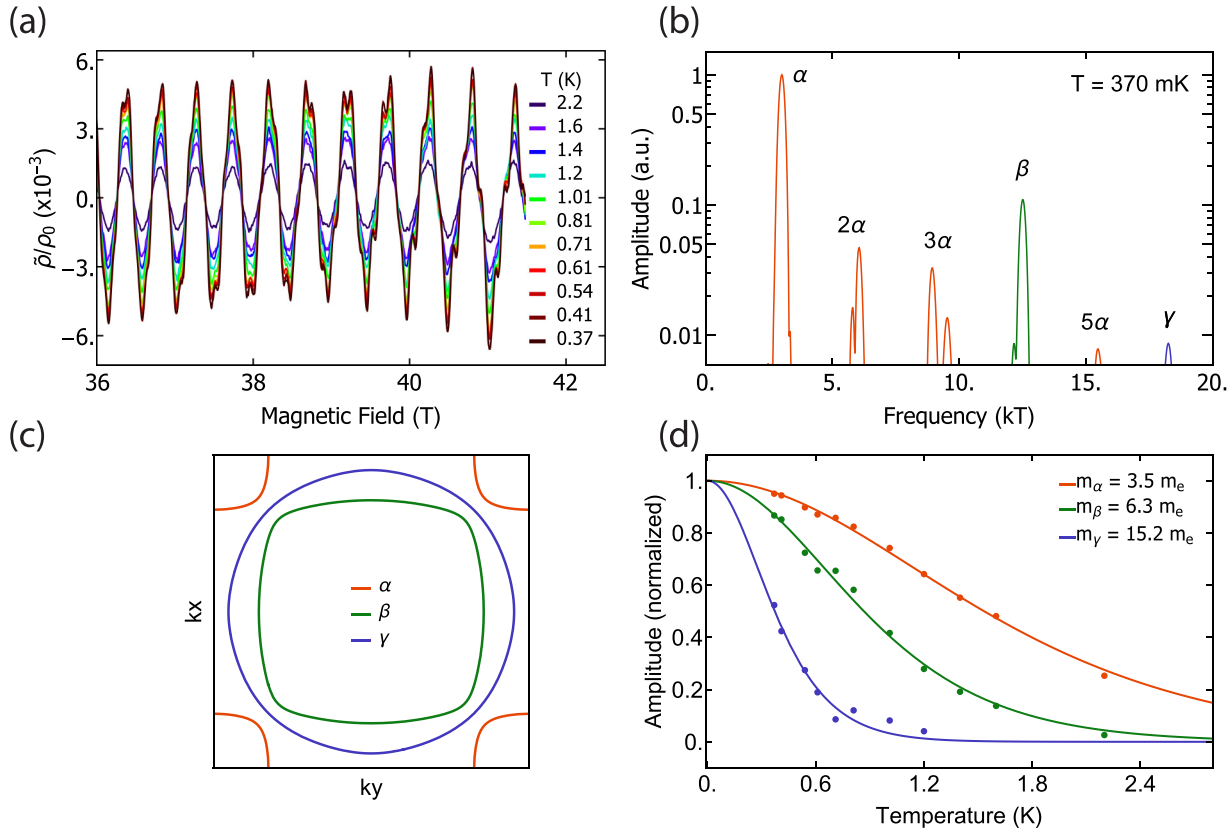

FIG. 2. Analysis of the Shubnikov–de Haas oscillations. (a) Temperature dependence of the Shubnikov–de Hass oscillations in the field range from 36 to 41.5 T. Additional frequency components—beyond the 3 kT frequency of the α pocket—become clearly visible at higher field. (b) Fast Fourier transform (FFT) of the 370 mK data. The primary frequencies corresponding to the α, β, and γ Fermi surfaces [shown in (c)] are indicated, as well as the higher harmonics of the α surface. The 4α harmonic overlaps with the beta frequency, but its contribution is roughly one order of magnitude smaller than that of the β frequency itself owing to the fact that each successive harmonic is damped more strongly than the last. (d) Temperature-dependent oscillation amplitude, with a fit to Eq. (2) for the α, β, and γ pockets. The analysis is done with data between 32 T and 41.5 T and from 370 mK to 2.2 K for α and β pockets, and between 35 T and 41.5 T and from 370 mK to 1.2 K for the γ pocket.

The quasiparticle effective mass $m^\star$ is obtained from the temperature dependence of the quantum oscillation amplitude. As the thermal energy (k_BT) becomes comparable to the cyclotron energy ($\hbar\omega_c$, where $\omega_c = \frac{eB}{m^\star}$), the oscillations are damped with the form

$$R_T = \left(2\pi^2 \frac{k_B T}{\hbar\omega_c}\right) \Big/ \sinh\left(2\pi^2 \frac{k_B T}{\hbar\omega_c}\right). \qquad (2)$$

Figure 2(d) shows fits of the FFT amplitude to Eq. (2). The effective mass for the α, β, and γ sheets are found to be $m^\star_\alpha = 3.5 \pm 0.1\ m_e$, $m^\star_\beta = 6.3 \pm 0.2\ m_e$, and $m^\star_\gamma = 15.2 \pm 1.3\ m_e$, where m_e is the bare electron mass. These masses are consistent with those found in single-crystal Sr_2RuO_4 (see Table I), which is also consistent with the similarity in measured Fermi surface areas. The consistency between these Fermi surface

TABLE I. A comparison of the Fermi surface parameters extracted for a Sr_2RuO_4 film grown on LSAT and those obtained from de Haas–van Alphen measurements on single-crystal Sr_2RuO_4 [18,19] (τ_q for single-crystals comes from Ref. [20]). The transport lifetime τ_t is calculated from the value of $\rho_{xx}(T_c)$ assuming that the ratio τ_t/τ_q is the same for all sheets of Fermi surface. The quantum lifetime is extracted from the data taken at $T = 370$ mK, which has oscillations from all three Fermi surfaces over the broadest field range. The details of the estimation of uncertainties are described in the supplementary information [16].

Fermi surface	Frequency (T)	Effective mass (m_e)	τ_q (ps) (Quantum lifetime)	τ_t (ps) (Transport lifetime)
α (film)	3079 ± 99	3.5 ± 0.1	1.07 ± 0.04	1.39 ± 0.12
α (single crystal)	3010 ± 80	3.4 ± 0.1	2.0	
β (film)	12510 ± 108	6.3 ± 0.2	0.66 ± 0.01	0.86 ± 0.07
β (single crystal)	12730 ± 150	6.8 ± 0.2	1.7	
γ (film)	18259 ± 195	15.2 ± 1.3	0.71 ± 0.07	0.92 ± 0.12
γ (single crystal)	18570 ± 70	14.0 ± 2.0	2.4	

parameters suggests that films of Sr_2RuO_4 grown on LSAT are close electronic analogs of the bulk material.

The remaining quantity to be determined is the quasiparticle quantum lifetime τ_q. As the inverse of the time between scattering events becomes comparable to the cyclotron frequency ω_c (or the Landau level widths becomes comparable to their separation), the oscillations are damped as

$$R_D = e^{-\frac{\pi}{\omega_c \tau_q}}. \quad (3)$$

The lifetime can be converted to a mean free path via $\tau_q = l_{free}/v_F$, where the Fermi velocity v_F is determined by the measured Fermi surface area and effective mass.

The quantum lifetime is more challenging to extract than the cyclotron mass and Fermi surface area for two reasons. First, the α pocket dominates the raw oscillatory signal, making it impossible to fit Eq. (3) directly to the data for the β and γ bands. Second, the presence of interlayer coupling leads to a beat-like structure in the data rather than a pure exponential envelope [17]. We solve the first problem by Fourier-filtering the data over frequency ranges that only include one FS component at a time. We solve the second by fitting the data over as broad a field-range as possible and by comparing the results of two different analyses to check for consistency.

We first extract the quantum lifetime with a Dingle plot. The Shubnikov–de Haas oscillation amplitude for a quasi-two-dimensional (2D) Fermi surface is given by

$$\frac{\widetilde{\rho}}{\rho_0} \propto R_T R_D \cos\left(\frac{2\pi F}{B}\right), \quad (4)$$

where R_T is given by Eq. (2) and R_D is given by Eq. (3). We first find the peaks of the oscillations in $|\widetilde{\rho}/\rho_0|$, divide the peak amplitude by R_T, and then plot the absolute value of this quantity on a log scale as a function of $1/B$; these plots are shown in Supplementary Fig. S2 [16]. With $m^\star$ determined from the temperature dependence, the quantum lifetimes can be immediately obtained from the slope of this plot.

The second method we use to determine the quantum lifetime is to directly fit the oscillations with Eq. (4)—these plots are shown in Supplementary Fig. S3 [16]. This has the advantage over the first technique of making use of the full data set, but as Eq. (4) ignores the interlayer dispersion (which cannot be clearly resolved over this field range), it can become contaminated by the beat structure.

The two methods give similar estimates for τ_q. We take the average of the two results and estimate the uncertainty as half of the difference between them. The quantum lifetimes of the α, β, and γ sheets are 1.07 ± 0.04 ps, 0.66 ± 0.01 ps, and 0.71 ± 0.07 ps, respectively. As the γ pocket was only observed above 35 T, there is certainly a larger systematic uncertainty associated with this lifetime than we are able to account for with this method. Converting the three lifetimes to mean free paths yields 108 nm, 75 nm, and 40 nm, for the α, β, and γ Fermi surfaces, respectively. These values can be compared with those obtained from single crystals: the authors of Ref. [20] reported Dingle temperatures that convert to mean free paths of 210 nm, 176 nm, and 130 nm, for the α, β, and γ Fermi surfaces, respectively. While the single-crystal values are somewhat longer than those from our film, the progression of the longest mean free path on the α pocket to the shortest on the γ pocket is consistent (note that subsequent generations of single-crystal Sr_2RuO_4 have even longer mean free paths [17]).

The transport lifetime τ_t—a quantity related to, but distinct from, the quantum lifetime—can be extracted from the absolute value of the resistivity ρ_{xx} now that the Fermi surface areas and effective masses are known. We start with a tight-binding model of Sr_2RuO_4's band structure [7], adjust the tight-binding parameters so that the Fermi surface areas and effective masses match the values measured for our sample, and then solve the Boltzmann transport equation using Chambers' solution [21] (details are given in the supplementary information [16]). As there are three transport lifetimes—one for each Fermi surface—but only one value of ρ_{xx} to fit, we make the simplifying assumption that the ratio of τ_t to τ_q is the same for all sheets of Fermi surface. We adjust this ratio until the calculated resistivity matches the measured residual resistivity, $\rho_{xx}(T_c)$=1 $\mu\Omega$ cm. We find that $\tau_t/\tau_q = 1.3 \pm 0.1$. This translates to transport mean free paths of 140 nm, 97 nm, and 52 nm, for the α, β, and γ Fermi surfaces, respectively. Because τ_q is a lower bound on τ_t, the ratio τ_t/τ_q must be at least 1. If we relax the constraint that τ_t/τ_q is the same for all Fermi surfaces, then at most two Fermi surfaces could have $\tau_t/\tau_q = 1$ and the third would have τ_t/τ_q greater than 1.3 (the exact value depends on which Fermi surface is chosen). Without further microscopic justification for why τ_t/τ_q might be different on different Fermi surfaces, the assumption that this ratio is the same for all Fermi surfaces is the simplest one that we can make.

IV. DISCUSSION

The transport lifetimes we measure here approach those of clean-limit, single-crystal Sr_2RuO_4 [9]. They are also comparable to what was reported in some of the earliest quantum oscillation measurements of single-crystal Sr_2RuO_4 [22]. To put our measured mean free path of over 100 nm in context with other oxide thin film superconductors, a useful comparison can be made with $Pr_{2-x}Ce_xCuO_{4\pm\delta}$, whose crystal structure is very similar to that of Sr_2RuO_4. High-field quantum oscillation studies on $Pr_{2-x}Ce_xCuO_{4\pm\delta}$ measured the mean free path to be only 6 nm [23], highlighting the extremely high quality of our Sr_2RuO_4 films.

Long mean free paths are crucial for observing the intrinsic T_c of Sr_2RuO_4: the authors of Ref. [9] found that 90 nm is the critical transport mean free path for superconductivity in Sr_2RuO_4—any shorter and the material does not superconduct; any longer and the T_c rises rapidly to $\approx$1.5 K. We find mean free paths longer than this length on the α and β bands, which are thought to dominate the superconductivity in Sr_2RuO_4 [24], and which is consistent with a T_c of 1.05 K for single-crystal Sr_2RuO_4 [9].

The difference between the measured quantum and transport lifetimes may offer a clue as to what is the dominate scattering mechanism in these films. The quantum lifetime is the average time a quasiparticle spends in a momentum eigenstate before scattering. The transport lifetime is the average time between scattering events that relax the quasiparticle momentum distribution function. When scattering is isotropic, as it is for point-scatterers, $\tau_q = \tau_t$. For extended defects, the

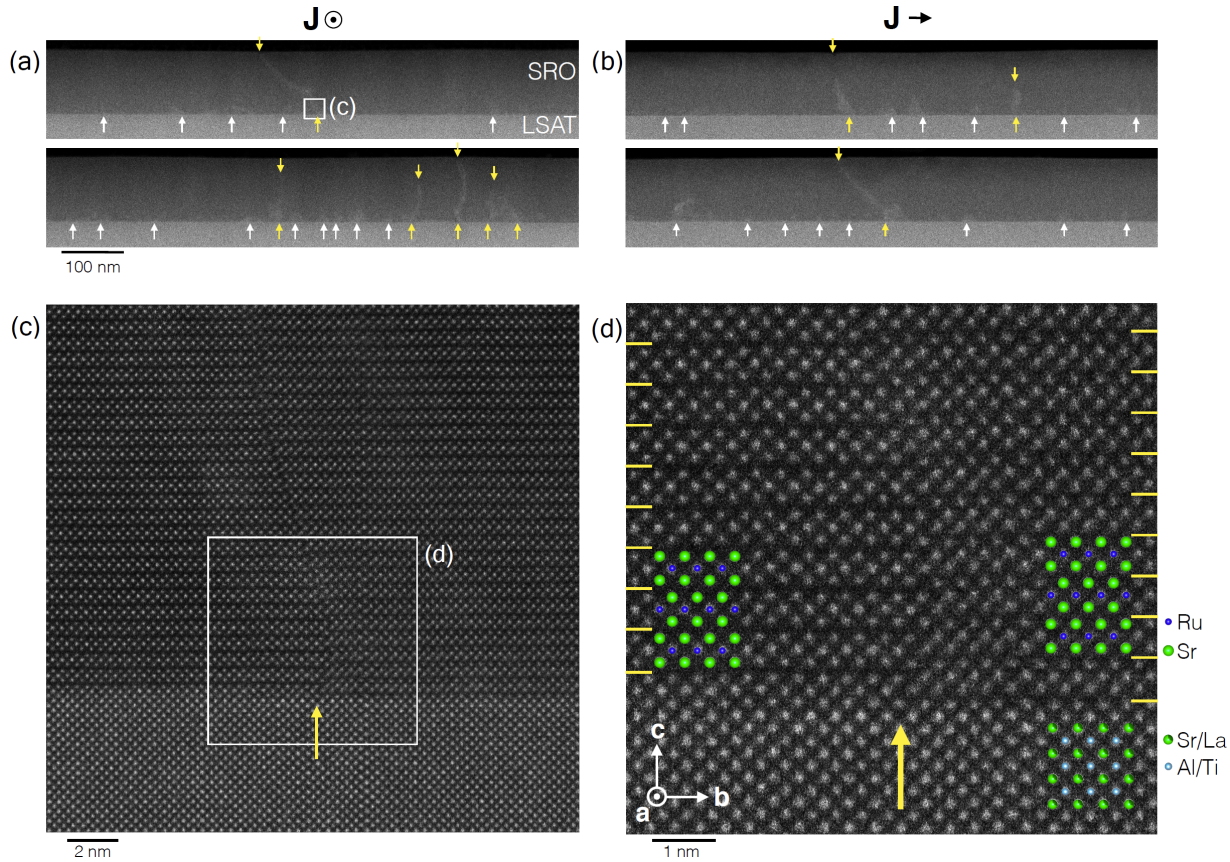

FIG. 3. Defect characterization by cross-sectional STEM. Atomic-resolution medium angle annular dark field scanning transmission electron microscopy (MAADF-STEM) images for cross sections (a) perpendicular and (b) parallel to the current direction in Fig. 1(a). Extended lattice defects, such as out-of-phase boundaries, are indicated with arrows. Many defects terminate near the interface of the film (white arrows), while some are observed to extend through more than half the film thickness (yellow arrows). (c) Nearly all out-of-phase boundaries can be traced to nucleate at step edges (yellow arrow) in the LSAT substrate surface, as seen in this atomic-resolution image of a defect nucleation from the region marked by the white box in (a). (d) High-magnification inset of the area marked by the white box in (c) shows how Sr_2RuO_4 layers growing near a single unit cell LSAT step edge meet at a vertical defect due to the vertical offset of SrO planes on either side of the step edge.

transport lifetime is generally longer than its quantum counterpart: extended defects contribute more forward-scattering events that do not alter the momentum distribution function of the quasiparticles but *do* decohere the quasiparticle wave functions. This was studied systematically in AlGaN/GaN heterostructures, where small-angle scattering from dislocations reduces the quantum lifetime by up to a factor of 20 below the transport lifetime [25]. While a ratio of 1.3 ± 0.1 is not nearly as compelling as a ratio of 20, we were nevertheless motivated to study the microscopic nature of the defects in this film.

To investigate the character and density of extended defects in our samples, we performed cross-sectional scanning transmission electron microscopy (STEM) on lamellas cut from the contact region of the device shown in Fig. 1(a). Figures 3(a) and 3(b) show representative cross sections cut parallel and perpendicular to the direction of the applied current, respectively (more images are shown in the Supplementary Information [16].) In the medium angle annular dark field (MAADF) collection geometry used here (40 mrad inner collection angle), extended defects—predominantly out-of-phase boundaries—are visible as regions of lighter contrast (yellow and white arrows). Some defects terminate near the interface (white arrows), while others extend through significant depth of the film (yellow arrows). These extended defects have a density of approximately 1 every 100 to 200 nm. This density is consistent with the quantum mean free path we extract from the quantum oscillations. The longer transport mean free path, as compared to the quantum mean free path, is consistent with the predominantly small-angle scattering that results from the large spatial extent of these defects [25]. Atomic-resolution MAADF-STEM images at the interface shown (autoreffig:stemc and d) show that step-edges in the LSAT substrate are predominant nucleation sites for these defects. A single unit cell step edge in the LSAT substrate surface appears at the base of a vertically running fault in the film, visible as offset SrO rock salt layers on either side (marked by yellow lines). This suggests that future improvements in Sr_2RuO_4 film quality should focus on reducing the density of step edges through substrate surface preparation.

The extreme sensitivity of T_c to disorder in Sr_2RuO_4 raises the question of whether the relatively high T_c observed in thin films can be attributed to film cleanliness or whether the presence of the substrate significantly modifies the electronic

structure and thus T_c. The Fermi surface areas and quasiparticle effective masses we measure for Sr_2RuO_4 grown on LSAT are the same as those found in single-crystal Sr_2RuO_4 to within our measurement uncertainty. This suggests that modifications to the electronic structure, such as an enhanced density of states (proportional to $m^\star$ in two-dimensional materials) due to substrate strain pushing the Fermi surface toward the van Hove point, are not responsible for the relatively high T_c (1.05 K) observed in these films grown on the commercial perovskite substrate that is best lattice matched to Sr_2RuO_4 [26]. It will be interesting to see how the electronic structure, mean free path, and perhaps even superconducting order parameter symmetry are modified when commensurately strained Sr_2RuO_4 films are grown on other substrates, where the T_c can be as high as 1.8 K and strain is undoubtedly playing a larger role [10].

ACKNOWLEDGMENTS

B.J.R. and Y.F. acknowledge support from the National Science Foundation under Grant No. DMR-1752784. A portion of this work was performed at the National High Magnetic Field Laboratory, which is supported by the National Science Foundation Cooperative Agreement No. DMR-1644779 and the State of Florida. H.P.N., L.M., N.J.S., B.H.G., L.F.K., K.M.S., and D.G.S. acknowledge support from the National Science Foundation [Platform for the Accelerated Realization, Analysis and Discovery of Interface Materials (PARADIM)] under Cooperative Agreement No. DMR-1539918. N.J.S. acknowledges support from the National Science Foundation Graduate Research Fellowship Program under Grant No. DGE-1650441. This research is funded in part by the Gordon and Betty Moore Foundation's EPiQS Initiative through Grants No. GBMF3850 and No. GBMF9073 to Cornell University. This work made use of the Cornell Center for Materials Research (CCMR) Shared Facilities, which are supported through the NSF MRSEC Program (No. DMR-1719875). Substrate preparation was performed in part at the Cornell NanoScale Facility, a member of the National Nanotechnology Coordinated Infrastructure (NNCI), which is supported by the NSF (Grant No. NNCI-2025233). The FEI Titan Themis 300 was acquired through Grant No. 1429155, with additional support from Cornell University, the Weill Institute, and the Kavli Institute at Cornell. The Thermo Fisher Helios G4 UX FIB was acquired with support by NSF Grant No. DMR-1539918. K.M.S. acknowledges support from NSF Grant No. DMR-1709255 and Air Force Office of Scientific Research Grant No. FA9550-15-1-0474.

[1] A. Pustogow, Y. Luo, A. Chronister, Y.-S. Su, D. A. Sokolov, F. Jerzembeck, A. P. Mackenzie, C. W. Hicks, N. Kikugawa, S. Raghu, E. D. Bauer, and S. E. Brown, Constraints on the superconducting order parameter in Sr_2RuO_4 from oxygen-17 nuclear magnetic resonance, Nature (London) **574**, 72 (2019).

[2] S. A. Kivelson, A. C. Yuan, B. Ramshaw, and R. Thomale, A proposal for reconciling diverse experiments on the superconducting state in Sr_2RuO_4, npj Quantum Mater. **5**, 43 (2020).

[3] S. Ghosh, A. Shekhter, F. Jerzembeck, N. Kikugawa, D. A. Sokolov, M. Brando, A. P. Mackenzie, C. W. Hicks, and B. J. Ramshaw, Thermodynamic evidence for a two-component superconducting order parameter in Sr_2RuO_4, Nat. Phys. **17**, 199 (2021).

[4] S. Raghu, A. Kapitulnik, and S. A. Kivelson, Hidden Quasi-One-Dimensional Superconductivity in Sr_2RuO_4, Phys. Rev. Lett. **105**, 136401 (2010).

[5] L.-D. Zhang, W. Huang, F. Yang, and H. Yao, Superconducting pairing in Sr_2RuO_4 from weak to intermediate coupling, Phys. Rev. B **97**, 060510(R) (2018).

[6] C. W. Hicks, D. O. Brodsky, E. A. Yelland, A. S. Gibbs, J. A. N. Bruin, M. E. Barber, S. D. Edkins, K. Nishimura, S. Yonezawa, Y. Maeno, and A. P. Mackenzie, Strong increase of Tc of Sr_2RuO_4 under both tensile and compressive strain, Science **344**, 283 (2014).

[7] B. Burganov, C. Adamo, A. Mulder, M. Uchida, P. D. C. King, J. W. Harter, D. E. Shai, A. S. Gibbs, A. P. Mackenzie, R. Uecker, M. Bruetzam, M. R. Beasley, C. J. Fennie, D. G. Schlom, and K. M. Shen, Strain Control of Fermiology and Many-Body Interactions in Two-Dimensional Ruthenates, Phys. Rev. Lett. **116**, 197003 (2016).

[8] S. Madhavan, D. G. Schlom, A. Dabkowski, H. A. Dabkowska, and Y. Liu, Growth of epitaxial *a*-axis and *c*-axis oriented Sr_2RuO_4 films, Appl. Phys. Lett. **68**, 559 (1996).

[9] A. P. Mackenzie, R. K. W. Haselwimmer, A. W. Tyler, G. G. Lonzarich, Y. Mori, S. Nishizaki, and Y. Maeno, Extremely Strong Dependence of Superconductivity on Disorder in Sr_2RuO_4, Phys. Rev. Lett. **80**, 161 (1998).

[10] H. P. Nair, J. P. Ruf, N. J. Schreiber, L. Miao, M. L. Grandon, D. J. Baek, B. H. Goodge, J. P. C. Ruff, L. F. Kourkoutis, K. M. Shen, and D. G. Schlom, Demystifying the growth of superconducting Sr_2RuO_4 thin films, APL Mater. **6**, 101108 (2018).

[11] M. Uchida, M. Ide, H. Watanabe, K. S. Takahashi, Y. Tokura, and M. Kawasaki, Molecular beam epitaxy growth of superconducting Sr_2RuO_4 films, APL Mater. **5**, 106108 (2017).

[12] C. M. P. Garcia, A. Di Bernardo, G. Kimbell, M. E. Vickers, F. C.-P. Massabuau, S. Komori, G. Divitini, Y. Yasui, H. G. Lee, J. Kim, B. Kim, M. G. Blamire, A. Vecchione, R. Fittipaldi, Y. Maeno, T. W. Noh, and J. W. A. Robinson, Pair suppression caused by mosaic-twist defects in superconducting Sr_2RuO_4 thin-films prepared using pulsed laser deposition, Commun. Mater. **1**, 23 (2020).

[13] M. A. Zurbuchen, Y. Jia, S. Knapp, A. H. Carim, D. G. Schlom, L.-N. Zou, and Y. Liu, Suppression of superconductivity by crystallographic defects in epitaxial Sr_2RuO_4 films, Appl. Phys. Lett. **78**, 2351 (2001).

[14] M. A. Zurbuchen, Y. Jia, S. Knapp, A. H. Carim, D. G. Schlom, and X. Q. Pan, Defect generation by preferred nucleation in epitaxial $Sr_2RuO_4/LaAlO_4$, Appl. Phys. Lett. **83**, 3891 (2003).

[15] D. Shoenberg, *Magnetic Oscillations in Metals* (Cambridge University Press, Cambridge, England, 1984).

[16] See Supplemental Material at http://link.aps.org/supplemental/10.1103/PhysRevB.104.045152 for details of the data processing and background removal, how we obtained the uncertainties in Table I, the two methods for extracting the quantum lifetime,

the method for calculating the residual resistivity, and more cross-sectional STEM images.

[17] C. Bergemann, A. P. Mackenzie, S. R. Julian, D. Forsythe, and E. Ohmichi, Quasi-two-dimensional fermi liquid properties of the unconventional superconductor Sr_2RuO_4, Adv. Phys. **52**, 639 (2003).

[18] C. Bergemann, S. R. Julian, A. P. Mackenzie, A. W. Tyler, D. E. Farrell, Y. Maeno, and S. Nishizaki, Quantum oscillations and overcritical torque interaction in Sr_2RuO_4, Physica C: Superconductivity **317-318**, 444 (1999).

[19] C. Bergemann, J. S. Brooks, L. Balicas, A. P. Mackenzie, S. R. Julian, Z. Q. Mao, and Y. Maeno, Normal state of the unconventional superconductor Sr_2RuO_4 in high magnetic fields, Phys. B: Condens. Matter **294-295**, 371 (2001).

[20] A. P. Mackenzie, S. R. Julian, A. J. Diver, G. J. McMullan, M. P. Ray, G. G. Lonzarich, Y. Maeno, S. Nishizaki, and T. Fujita, Quantum Oscillations in the Layered Perovskite Superconductor Sr_2RuO_4, Phys. Rev. Lett. **76**, 3786 (1996).

[21] R. G. Chambers, The kinetic formulation of conduction problems, Proc. Phys. Soc. A **65**, 458 (1952).

[22] A. P. Mackenzie, S. R. Julian, A. J. Diver, G. G. Lonzarich, N. E. Hussey, Y. Maeno, S. Nishizaki, and T. Fujita, Calculation of thermodynamic and transport properties of Sr2RuO4 at low temperatures using known Fermi surface parameters, Physica C: Superconductivity **263**, 510 (1996).

[23] N. P. Breznay, I. M. Hayes, B. J. Ramshaw, R. D. McDonald, Y. Krockenberger, A. Ikeda, H. Irie, H. Yamamoto, and J. G. Analytis, Shubnikov-de haas quantum oscillations reveal a reconstructed Fermi surface near optimal doping in a thin film of the cuprate superconductor $Pr_{1.86}Ce_{0.14}CuO_{4\pm\delta}$, Phys. Rev. B **94**, 104514 (2016).

[24] R. Sharma, S. D. Edkins, Z. Wang, A. Kostin, C. Sow, Y. Maeno, A. P. Mackenzie, J. C. S. Davis, and V. Madhavan, Momentum-resolved superconducting energy gaps of Sr_2RuO_4 from quasiparticle interference imaging, Proc. Natl. Acad. Sci. USA **117**, 5222 (2020).

[25] M. J. Manfra, S. H. Simon, K. W. Baldwin, A. M. Sergent, K. W. West, R. J. Molnar, and J. Caissie, Quantum and transport lifetimes in a tunable low-density algan/gan two-dimensional electron gas, Appl. Phys. Lett. **85**, 5278 (2004).

[26] D. G. Schlom, L.-Q. Chen, C. J. Fennie, V. Gopalan, D. A. Muller, X. Pan, R. Ramesh, and R. Uecker, Elastic strain engineering of ferroic oxides, MRS Bull. **39**, 118 (2014).